Medicinal Chemistry Research (2019) 28:81–94
https://doi.org/10.1007/s00044-018-2266-x

MEDICINAL CHEMISTRY RESEARCH

ORIGINAL RESEARCH

Design, synthesis, and biological evaluation of indole carboxylic acid esters of podophyllotoxin as antiproliferative agents

Lei Zhang[1] · Xian Zeng[1] · Xiaodong Ren[2] · Nengyin Tao[1] · Chengli Yang[1,3] · Yingshu Xu[1] · Yongzheng Chen[1] · Jing Wang[1]

Received: 30 August 2018 / Accepted: 15 November 2018 / Published online: 26 November 2018

Abstract

A series of indole carboxylic acid conjugates of the podophyllotoxin were synthesized and evaluated as antiproliferative agents against two human chronic myeloid leukemia cell lines. Several compounds (**In-2**, **In-8** and **In-9**) not only showed antiproliferative activity against normal K562 cells but also exhibited potent antineoplastic effect against resistant K562/VCR cells. The indole-6-formyl conjugate, **In-9**, revealed potent cytotoxic activity against K562 and K562/VCR cell lines, with IC_{50} values of 0.100 ± 0.008 and 0.227 ± 0.011 μM, respectively. Preliminary mechanism studies indicated that **In-9** could disrupt the microtubule network in K562/VCR cells via occupying the colchicine binding site of the tubulin. Molecular dynamics simulation results revealed that the complex of **In-9** and tubulin were stable. Furthermore, **In-9** induced intracellular ROS generation, apoptosis, and cycle arrest at the G2 phase by inhibition of CDKs, loss of mitochondrial membrane potential and cleavage of caspase. **In-9** simultaneously induced K562/VCR cells autophagy by upregulating the levels of Beclin1 and LC3-II, and exhibited anti-MDR ability by downregulating the levels of P-gp and MRP1. Finally, **In-9** activated the AMPK and JNK signaling, and inhibited the ERK, P38, and PI3K/AKT/mTOR signaling in K562/VCR cells. In silico prediction indicated that **In-9** mainly obeyed Lipinski rule for druglikeness. Together, **In-9** possessed potent antiproliferative activity, and may be a promising agent for the potential treatment of resistant leukemia cancer.

Keywords Podophyllotoxin · Indole carboxylic acid · Anti-MDR activity · Apoptosis · Autophagy

Introduction

Multidrug resistance (MDR) remains the major clinical impediment in carcinoma chemotherapy (Gottesman 2002). Mechanisms involved in MDR have been intensively studied, and appear to be quite complex, such as drug efflux, cell cycle checkpoint, metabolism, and microenvironment (Szakács et al. 2006). In cancer cells, one of the most prominent causes of MDR is overexpression of ATP-binding cassette (ABC) transporters (Shukla et al. 2008). ABC transporters, members of transport system superfamily, are involved in efflux of toxic molecules and xenobiotics out of the cell by using the energy of ATP hydrolysis. The most well-known drug transporter is P-glycoprotein (P-gp), which is encoded by MDR1 gene and plays a key function in the progress of MDR in cancer (Aller et al. 2009). Therefore, blocking P-gp transporter function or inhibiting P-gp expression might be effectively strategy to overcome MDR and treat MDR cancer (Li et al. 2016). Over the past few decades, considerable efforts have been made to develop novel and efficient P-gp inhibitors,

Electronic supplementary material The online version of this article (https://doi.org/10.1007/s00044-018-2266-x) contains supplementary material, which is available to authorized users.

✉ Lei Zhang
lzhang@zmc.edu.cn

✉ Jing Wang
wangjing@zmc.edu.cn

[1] Generic Drug Research Center of Guizhou Province, Green Pharmaceuticals Engineering Research Center of Guizhou Province, School of Pharmacy, Zunyi Medical University, 563003 Zunyi, China

[2] Department of Pharmacy, Guizhou Provincial People's Hospital, 550002 Guiyang, China

[3] State Key Laboratory of Biotherapy/Collaborative Innovation Center of Biotherapy, West China Hospital, Sichuan University, 610041 Chengdu, China

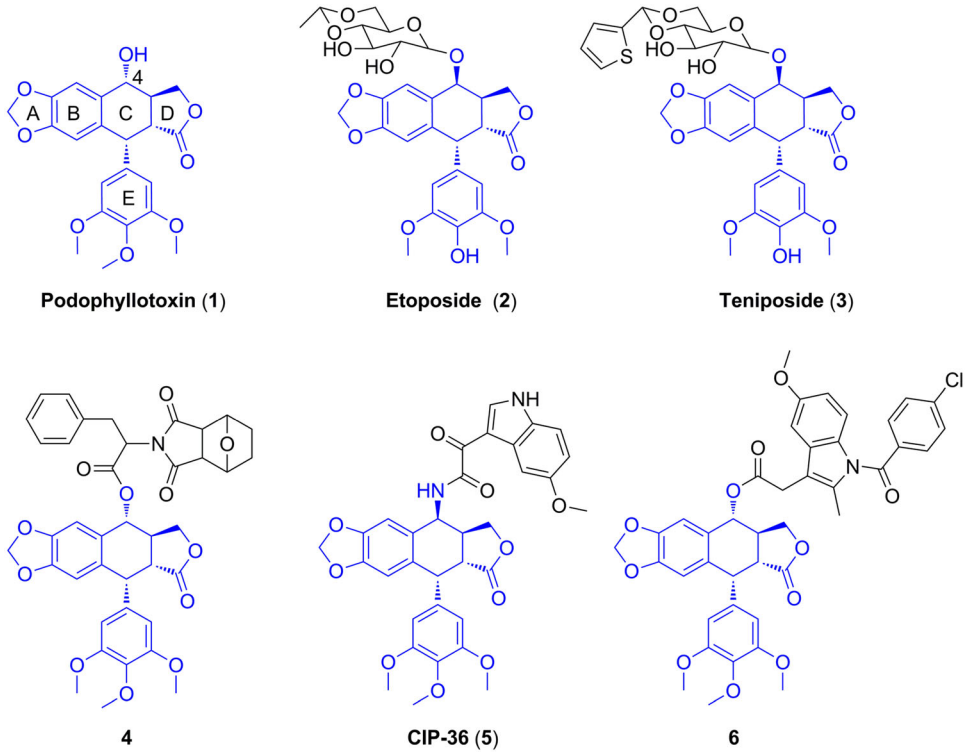

Fig. 1 The structures of podophyllotoxin and its derivatives

such as third-generation P-gp inhibitors, HM30181, WK-X-34, and tariquidar with great affinity to P-gp at a nM concentration (Binkhathlan and Lavasanifar 2013). However, no one P-gp inhibitor has been approved for use in clinic due to side effects, pharmacokinetic interaction and low clinical efficacy (Kathawala et al. 2015). On the other hand, recent studies showed that the inhibition of P-gp protein expression was efficacious in overcoming MDR in various cancer cell lines (Chen et al. 2010; Cheng et al. 2014).

Podophyllotoxin (**1**, Fig. 1), a well-known naturally occurring cyclolignan isolated from *Podophyllum peltatum* and *Podophyllum hexandrum*, exhibits cathartic, antirheumatic, antiviral, pesticidal, and antitumor properties. Etoposide (**2**, Fig. 1) and teniposide (**3**, Fig. 1) are semisynthetic glucosidic derivatives of podophyllotoxin widely used for the chemotherapy of various cancer types, including lymphoma, small-cell lung cancer, neuroblastoma, testicular carcinoma, and Kaposi's sarcoma (Baldwin et al. 2005). It was reported that podophyllotoxin could inhibit the assembly of tubulin, however, the two clinic drugs, etoposide and teniposide, were found to target DNA topoisomerase II via stabilizating the transient DNA topoisomerase II cleavage complex (Bailly 2012). Many evidences have indicated that etoposide and teniposide present several problems such as poor water solubility, moderate potency, drug resistance, and toxic effects (You 2005). Structure-activity relationship (SAR) studies have demonstrated that C-4 area of podophyllotoxin could be tolerant to significant structural diversification, such as aromatic and heterocyclic substituents (Kamal et al. 2015). Han and coworkers prepared a series of podophyllotoxin derivative at the C-4 hydroxyl groups by introducing various norcantharidin moieties. Among them, compound **4** (Fig. 1) was identified as the most potent molecule against MCF-7 cells with an IC_{50} value of 0.88 μM. Additionally, **4** could cause cell cycle arrest at G2/M phase, induce apoptosis, and inhibit microtubules polymerization (Han et al. 2016). Interestingly and importantly, many studies have demonstrated that the modification at the C-4 position of podophyllotoxin could improve anticancer activity against MDR cancer cell lines (Liu et al. 2013; Merzouki et al. 2012). For example, **CIP-36** (**5**, Fig. 1) has been reported by Cao et al. to overcome the MDR of multidrug-resistant K562/ADR cancer cell line via inhibiting Topo IIα activity (Cao et al. 2015). Over the past several years, our group have synthesized a series of podophyllotoxin derivatives containing various moieties with improved anticancer activity against MDR cells (Wang et al. 2018; Zhang et al. 2016a, b). For instance, we demonstrated that compound **6** (Fig. 1), a novel podophyllotoxin-indomethacin conjugate, not only showed antitumor activity against Bel-7402 cells but also significantly inhibited the proliferation of resistant Bel-7402/5-FU cells. Moreover, **6** exhibited less toxicity to human liver L-O2 cells in vitro (Zhang et al. 2017a).

Indole, an aromatic heterocyclic compound, is a ubiquitous core in bioactive natural products, as well as synthetic drugs, including vincristine, sunitinib, indirubin (**7**, Fig. 2), and midostaurin (**8**, Fig. 2) (Dadashpour and Emami

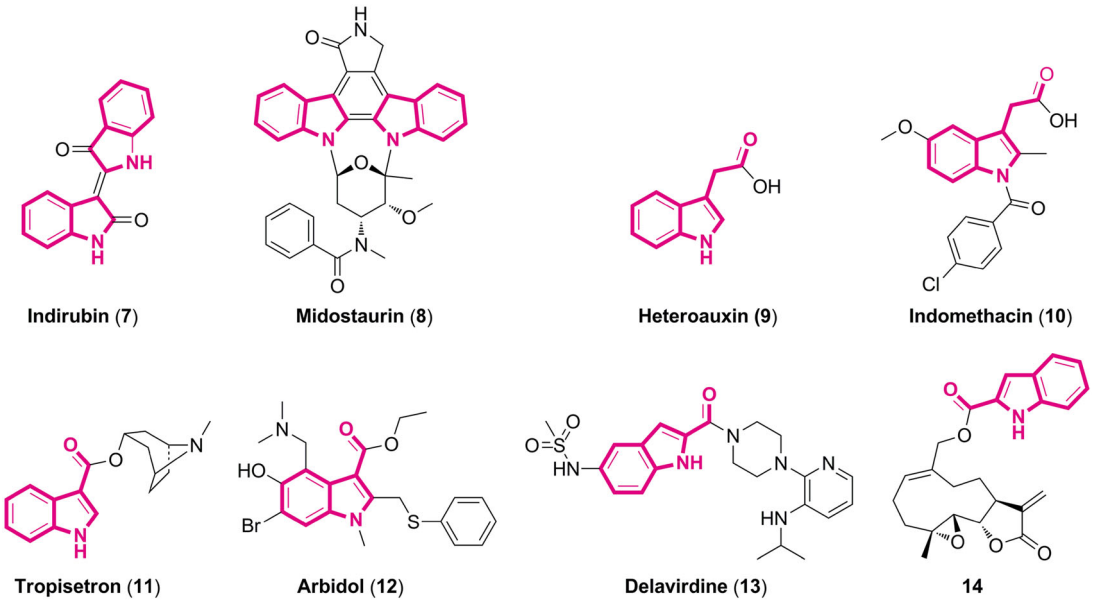

Fig. 2 Examples of natural products and pharmaceuticals with indole or indole carboxylic acid core highlighted

2018). For example, indirubin, a chemical constituent of indigo naturalis, has been used for many years in traditional Chinese medicine for treatment of chronic myelogenous leukemia. Recently, researches confirmed that indirubin and its derivative not only exhibited anticancer activity but also showed anti-inflammatory property (Lai et al. 2017; Zhang et al. 2017b). Additionally, midostaurin, a semisynthetic derivative of staurosporine, is a multi-targeted protein kinase inhibitor, which has been approved by FDA in 2017 for the treatment of acute myeloid leukemia (Stone et al. 2018). Furthermore, some reports showed that indole-3-carboxylic acid and its esters are also important motifs widely present in numerous natural bioactive compounds and pharmaceuticals, such as heteroauxin (**9**, Fig. 2), indomethacin (**10**, Fig. 2), tropisetron (**11**, Fig. 2), arbidol (**12**, Fig. 2), and delavirdine (**13**, Fig. 2) (Kim et al. 2010; Leneva et al. 2009; Romero et al. 1996). For example, arbidol showed broad spectrum antiviral activity, and was used for the prophylactic prevention and therapy of influenza A and B virus. As a first generation non-nucleoside reverse transcriptase inhibitor, delavirdine was approved for the therapy of human immunodeficiency virus type 1 (HIV-1). More recently, Bommagani et al. prepared a series of aryl carboxylic acid conjugates of sesquiterpene melampomagnolide-B. The indole-2-carboxylic acid conjugate **14** (Fig. 2) exhibited significantly improved anticancer activity against HCT-116 colon cancer cells (GI_{50} = 0.19 μM) when compared to parthenolide (Bommagani et al. 2017).

Molecular modeling analysis of previous studies had indicated that the introduction of moderate substituent at the C-4 hydroxyl resulted in a significant improved cytotoxic activity, which could insert into a hydrophobic cavity of α-Tubulin (Wang et al. 2017; Zhang et al. 2018). In present study, a series of podophyllotoxin derivatives bearing indole carboxylic acid fragment at C-4 hydroxyl position, which reduce the volume of 4-chlorobenzoyl substituent, and change the distance & position of carboxylic group in compound **6** reported by our research group, were designed by using the molecular hybridization approach (Fig. 3) (Mishra and Singh 2016). The designed molecules might accommodate deeply the colchicine binding site of the β-tubulin and simultaneously occupy the hydrophobic cavity of α-Tubulin. To verify above hypothesis, we further examined its effect on the microtubule network using immunofluorescence assay, and the binding mode to tubulin was performed by molecular modeling. Furthermore, their antitumor activity and MDR reverting ability were evaluated against human K562 and/or vincristine-resistant K562/VCR cancer cells in vitro.

Materials and methods

Chemistry

Melting points were obtained using a microscope melting-point apparatus (SGWX-4). Proton and carbon NMR spectra were detected on an Agilent spectrometer at 400 and 100 MHz, respectively. High-resolution mass spectra were recorded on an Agilent TOF-MS 6520. Reactions were monitored by thin layer chromatography on silica gel GF254 plates. Column chromatography was performed on silica gel (200–300 mesh).

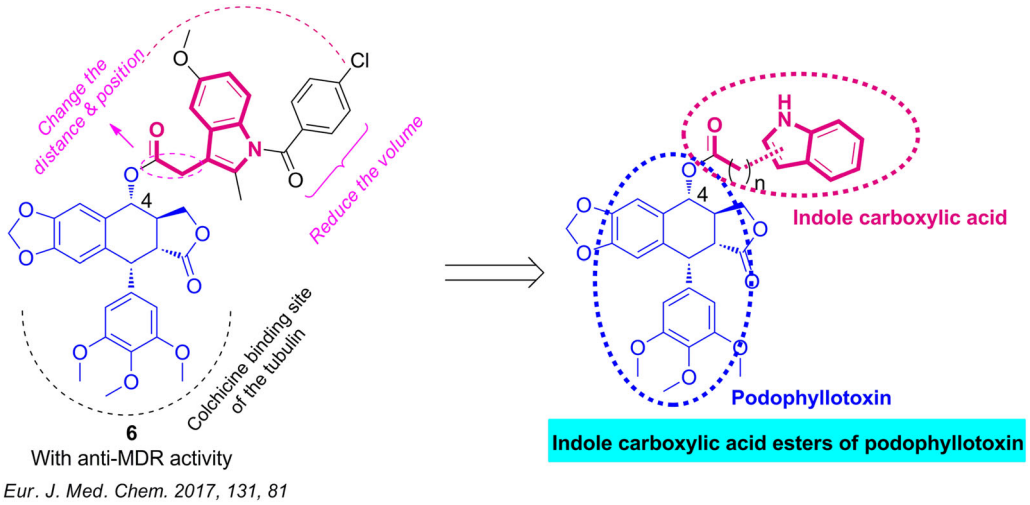

Fig. 3 Design of the indole carboxylic acid esters of podophyllotoxin

General procedure for the preparation of compounds In-1-In-10

To a solution of podophyllotoxin (0.29 mmol, 1 eq), appropriate indole carboxylic acid (1.5 eq), 4-dimethylamino-pyridine (1.2 eq) in N,N-dimethylformamide (4 mL) at 0 °C, 1-(3-dimethylaminopropyl)-3-ethylcarbodiimide hydrochloride (2 eq) was added. After stirring for 2–8 h at room temperature under argon atmosphere, the mixture was quenched with H_2O and the crude was collected by vacuum filtration, washed by water and dried in vacuum oven. The crude product was further purified by column chromatography (EtOAc/PE, 4:1) to provide the pure product.

4α-(indole-2-formyl)-4-desoxy-podophyllotoxin (***In-1***) White solid, yield 62%; mp: 151–153 °C; ^{1}H NMR (400 MHz, $CDCl_3$) δ 9.06 (s, 1 H), 7.70 (d, J = 8.0 Hz, 1 H), 7.45 (d, J = 8.4 Hz, 1 H), 7.36 (t, J = 8.0 Hz, 1 H), 7.25 (s, 1 H), 7.18 (t, J = 7.2 Hz, 1 H), 6.90 (s, 1 H), 6.58 (s, 1 H), 6.46 (s, 2 H), 6.13 (d, J = 7.2 Hz, 1 H), 6.00 (d, J = 8.0 Hz, 2 H), 4.65 (s, 1 H), 4.47 (t, J = 7.2 Hz, 1 H), 4.30 (t, J = 8.8 Hz, 1 H), 3.81 (s, 3 H), 3.80 (s, 6 H), 3.07–2.96 (m, 2 H); ^{13}C NMR (100 MHz, $CDCl_3$) δ 173.65, 162.28, 152.67, 148.26, 147.72, 137.25, 134.80, 132.47, 128.21, 127.29, 126.12, 126.07, 122.70, 121.23, 112.01, 109.81, 109.61, 108.22, 107.07, 101.64, 74.26, 71.41, 60.75, 56.22, 45.60, 43.78, 38.75; HRMS-ESI (*m/z*): calcd for $C_{31}H_{27}NNaO_9$ $[M + Na]^+$ 580.1578, found 580.1576.

4α-(indole-3-acetyl)-4-desoxy-podophyllotoxin (***In-2***) White solid, yield 72%; mp: 117–118 °C; ^{1}H NMR (400 MHz, $CDCl_3$) δ 8.26 (s, 1 H), 7.60 (d, J = 7.6 Hz, 1 H), 7.38 (d, J = 8.0 Hz, 1 H), 7.20 (t, J = 8.0 Hz, 2 H), 7.11 (t, J = 7.6 Hz, 1 H), 6.67 (s, 1 H), 6.51 (s, 1 H), 6.37 (s, 2 H), 5.98 (d, J = 9.2 Hz, 2 H), 5.88 (d, J = 8.8 Hz, 1 H), 4.57 (d, J = 4.4 Hz, 1 H), 4.21–4.11 (m, 2 H), 3.89 (s, 2 H), 3.81 (s, 3 H), 3.72 (s, 6 H), 2.90–2.79 (m, 2 H); ^{13}C NMR (100 MHz, $CDCl_3$) δ 173.66, 172.50, 152.59, 148.08, 147.52, 137.08, 136.13, 134.86, 132.22, 128.25, 126.88, 123.00, 122.50, 119.85, 118.49, 111.41, 109.62, 108.07, 107.84, 107.06, 101.54, 73.97, 71.31, 60.75, 56.12, 45.47, 43.71, 38.61, 31.61, 14.19; HRMS-ESI (*m/z*): calcd for $C_{32}H_{29}NNaO_9$ $[M + Na]^+$ 594.1738, found 594.1735.

4α-(2-methylindole-3-acetyl)-4-desoxy-podophyllotoxin (***In-3***) White solid, yield 79%; mp: 118–120 °C; ^{1}H NMR (400 MHz, $CDCl_3$) δ 8.07 (s, 1 H), 7.50 (d, J = 6.4 Hz, 1 H), 7.25 (s, 1 H), 7.11 (s, 1 H), 7.05 (s, 1 H), 6.58 (s, 1 H), 6.49 (s, 1 H), 6.36 (s, 2 H), 5.98 (s, 1 H), 5.94 (s, 1 H), 5.81 (d, J = 8.4 Hz, 1 H), 4.55 (s, 1 H), 4.12–4.06 (m, 2 H), 3.82 (s, 3 H), 3.78 (s, 2 H), 3.72 (s, 6 H), 2.85–2.76 (m, 2 H), 2.41 (s, 3 H); ^{13}C NMR (100 MHz, $CDCl_3$) δ 173.70, 172.46, 152.57, 148.03, 147.49, 137.04, 135.12, 134.93, 132.66, 132.12, 128.34, 128.06, 121.54, 119.70, 117.67, 110.51, 109.58, 108.04, 106.95, 103.93, 101.53, 73.84, 71.26, 60.74, 56.07, 45.38, 43.69, 38.57, 30.68, 11.70; HRMS-ESI (*m/z*): calcd for $C_{33}H_{31}NNaO_9$ $[M + Na]^+$ 608.1891, found 608.1891.

4α-(indole-3-propionyl)-4-desoxy-podophyllotoxin (***In-4***) White solid, yield 75%; mp: 107–108 °C; ^{1}H NMR (400 MHz, $CDCl_3$) δ 8.13 (s, 1 H), 7.59 (d, J = 7.6 Hz, 1 H), 7.35 (d, J = 8.4 Hz, 1 H), 7.18 (t, J = 8.0 Hz, 1 H), 7.10 (t, J = 7.6 Hz, 1 H), 7.03 (s, 1 H), 6.52 (d, J = 6.4 Hz, 2 H), 6.35 (s, 2 H), 5.96 (s, 2 H), 5.83 (d, J = 9.6 Hz, 1 H), 4.56 (d, J = 4.4 Hz, 1 H), 4.10 (d, J = 8.8 Hz, 2 H), 3.81 (s, 3 H), 3.73 (s, 6 H), 3.17 (t, J = 7.2 Hz, 2 H), 2.87–2.82 (m, 3 H), 2.72–2.62 (m, 1 H); ^{13}C NMR (100 MHz, $CDCl_3$) δ 173.83, 173.70, 152.57, 148.02, 147.46, 137.12, 136.26, 134.87, 132.19, 128.29, 126.92, 122.25, 121.49, 119.44, 118.49, 114.24, 111.34, 109.60, 108.12, 107.01, 101.53, 73.46,

71.27, 60.76, 56.19, 45.52, 43.66, 38.60, 35.18, 20.89; HRMS-ESI (*m/z*): calcd for $C_{33}H_{31}NNaO_9$ $[M + Na]^+$ 608.1891, found 608.1889.

4α-((2 S)-2-N-((tert-Butoxy)carbonyl)-1H-indol-3-propionyl)-4-desoxy-podophyllotoxin (***In-5***) White solid, yield 69%; mp: 134–136 °C; ^{1}H NMR (400 MHz, $CDCl_3$) δ 8.28 (s, 1 H), 7.54 (d, $J = 8.0$ Hz, 1 H), 7.31 (d, $J = 8.0$ Hz, 1 H), 7.15 (t, $J = 8.0$ Hz, 1 H), 7.03 (s, 1 H), 6.99 (t, $J = 7.2$ Hz, 1 H), 6.51 (d, $J = 9.6$ Hz, 2 H), 6.35 (s, 2 H), 5.98 (d, $J = 5.6$ Hz, 2 H), 5.79 (d, $J = 9.2$ Hz, 1 H), 5.13 (d, $J = 7.2$ Hz, 1 H), 4.73 (d, $J = 6.8$ Hz, 1 H), 4.55 (d, $J = 4.4$ Hz, 1 H), 3.94 (t, $J = 10.0$ Hz, 1 H), 3.82 (s, 3 H), 3.74 (s, 6 H), 3.31 (d, $J = 4.8$ Hz, 2 H), 2.83 (dd, $J = 4.4$, 14.4 Hz, 1 H), 2.57–2.47 (m, 1 H), 1.66 (s, 1 H), 1.44 (s, 9 H); ^{13}C NMR (100 MHz, $CDCl_3$) δ 173.62, 172.93, 155.19, 152.58, 148.14, 147.57, 137.23, 136.05, 134.94, 132.15, 127.81, 127.14, 122.62, 119.80, 118.43, 111.43, 109.53, 108.22, 107.22, 101.56, 80.30, 74.47, 71.11, 60.77, 60.39, 56.27, 54.69, 45.53, 43.57, 38.40, 28.29, 27.86, 14.19; HRMS-ESI (*m/z*): calcd for $C_{38}H_{40}N_2NaO_{11}$ $[M + Na]^+$ 723.2524, found 723.2525.

4α-((2 R)-2-N-((tert-Butoxy)carbonyl)-1H-indol-3-propionyl)-4-desoxy-podophyllotoxin (***In-6***) White solid, yield 72%; mp: 132–134 °C; ^{1}H NMR (400 MHz, $CDCl_3$) δ 8.32 (s, 1 H), 7.60 (d, $J = 7.6$ Hz, 1 H), 7.38 (d, $J = 8.4$ Hz, 1 H), 7.18 (t, $J = 8.0$ Hz, 1 H), 7.11 (s, 1 H), 7.09 (d, $J = 8.0$ Hz, 1 H), 6.46 (s, 1 H), 6.30 (s, 2), 6.07 (s, 1 H), 5.95 (d, $J = 4.0$ Hz, 2 H), 5.77 (d, $J = 9.2$ Hz, 1 H), 5.04 (d, $J = 5.6$ Hz, 1 H), 4.60 (q, $J = 6.8$ Hz, 1 H), 4.53 (d, $J = 3.6$ Hz, 1 H), 4.13–4.05 (m, 1 H), 3.81 (s, 3 H), 3.71 (s, 6 H), 3.30 (d, $J = 6.4$ Hz, 2 H), 2.84–2.72 (m, 2 H), 1.68 (s, 1 H), 1.41 (s, 9 H); ^{13}C NMR (100 MHz, $CDCl_3$) δ 173.72, 152.56, 147.97, 147.30, 137.08, 136.25, 134.79, 132.24, 127.78, 127.18, 122.70, 122.51, 119.83, 118.48, 111.59, 109.99, 109.51, 108.06, 106.99, 101.46, 74.31, 71.34, 60.75, 56.16, 54.90, 45.49, 43.62, 38.56, 28.26, 28.04, 14.19; HRMS-ESI (*m/z*): calcd for $C_{38}H_{40}N_2NaO_{11}$ $[M + Na]^+$ 723.2524, found 723.2526.

4α-(indole-3-butyryl)-4-desoxy-podophyllotoxin (***In-7***) White solid, yield 65%; mp: 102–104 °C; ^{1}H NMR (400 MHz, $CDCl_3$) δ 8.07 (s, 1 H), 7.60 (d, $J = 8.0$ Hz, 1 H), 7.35 (d, $J = 8.0$ Hz, 1 H), 7.19 (t, $J = 8.0$ Hz, 1 H), 7.10 (t, $J = 7.6$ Hz, 1 H), 6.98 (s, 1 H), 6.74 (s, 1 H), 6.54 (s, 1 H), 6.38 (s, 2 H), 5.98 (s, 2 H), 5.87 (d, $J = 9.2$ Hz, 1 H), 4.60 (d, $J = 4.0$ Hz, 1 H), 4.29 (t, $J = 7.6$ Hz, 1 H), 4.17 (t, $J = 9.2$ Hz, 1 H), 3.81 (s, 3 H), 3.73 (s, 6 H), 2.88–2.84 (m, 3 H), 2.81–2.70 (m, 1 H), 2.56–2.42 (m, 2 H), 2.14–2.07 (m, 2 H); ^{13}C NMR (100 MHz, $CDCl_3$) δ 174.12, 173.70, 152.60, 148.08, 147.55, 137.11, 136.36, 134.88, 132.29, 128.38, 127.27, 122.07, 121.59, 119.29, 118.71, 115.02, 111.19, 109.67, 108.09, 107.09, 101.58, 73.43, 71.43, 60.77, 56.15, 45.60, 43.70, 38.75, 33.79, 25.31, 24.51; HRMS-ESI (*m/z*): calcd for $C_{34}H_{33}NNaO_9$ $[M + Na]^+$ 622.2048, found 622.2044.

4α-(indole-5-formyl)-4-desoxy-podophyllotoxin (***In-8***) White solid, yield 71%; mp: 138–140 °C; ^{1}H NMR (400 MHz, $CDCl_3$) δ 8.63 (s, 1 H), 8.41 (s, 1 H), 7.91 (d, $J = 8.0$ Hz, 1 H), 7.45 (d, $J = 8.0$ Hz, 1 H), 7.31 (s, 1 H), 6.94 (s, 1 H), 6.65 (s, 1 H), 6.59 (s, 1 H), 6.49 (s, 2 H), 6.15 (s, 1 H), 6.01 (d, $J = 10.8$ Hz, 2 H), 4.66 (s, 1 H), 4.49 (s, 1 H), 4.35 (s, 1 H), 3.80 (s, 9 H), 3.02 (s, 2 H); ^{13}C NMR (100 MHz, $CDCl_3$) δ 173.93, 167.86, 152.61, 148.10, 147.67, 138.73, 137.04, 135.03, 132.36, 128.92, 127.57, 126.02, 123.97, 123.26, 120.80, 111.05, 109.68, 108.09, 107.35, 103.99, 101.56, 73.60, 71.77, 60.76, 56.12, 45.72, 43.85, 39.03, 29.69; HRMS-ESI (*m/z*): calcd for $C_{31}H_{27}NNaO_9$ $[M + Na]^+$ 580.1578, found 580.1581.

4α-(indole-6-formyl)-4-desoxy-podophyllotoxin (***In-9***) White solid, yield 70%; mp: 153–155 °C; ^{1}H NMR (400 MHz, $CDCl_3$) δ 8.73 (s, 1 H), 8.18 (s, 1 H), 7.80 (d, $J = 8.4$ Hz, 1 H), 7.68 (d, $J = 8.4$ Hz, 1 H), 7.41 (s, 1 H), 6.93 (s, 1 H), 6.62 (s, 1 H), 6.59 (s, 1 H), 6.48 (s, 2 H), 6.13 (d, $J = 8.0$ Hz, 1 H), 5.99 (d, $J = 8.4$ Hz, 2 H), 4.65 (s, 1 H), 4.50–4.47 (m, 1 H), 4.37–4.32 (m, 1 H), 3.80 (s, 3 H), 3.78 (s, 6 H), 3.04–2.96 (m, 2 H); ^{13}C NMR (100 MHz, $CDCl_3$) δ 173.93, 167.90, 152.61, 148.11, 147.66, 137.07, 135.13, 135.01, 132.36, 132.14, 128.83, 128.23, 122.48, 120.64, 120.51, 113.76, 109.71, 108.14, 107.27, 103.12, 101.57, 73.81, 71.75, 60.75, 56.14, 45.69, 43.82, 38.98; HRMS-ESI (*m/z*): calcd for $C_{31}H_{27}NNaO_9$ $[M + Na]^+$ 580.1578, found 580.1580.

4α-(indole-7-formyl)-4-desoxy-podophyllotoxin (***In-10***) White solid, yield 68%; mp: 134–136 °C; ^{1}H NMR (400 MHz, $CDCl_3$) δ 9.87 (s, 1 H), 7.93 (d, $J = 7.6$ Hz, 1 H), 7.87 (d, $J = 7.2$ Hz, 1 H), 7.34 (s, 1 H), 7.18–7.14 (m, 1 H), 6.93 (s, 1 H), 6.64 (s, 1 H), 6.60 (s, 1 H), 6.46 (s, 2 H), 6.19 (s, 1 H), 6.01 (d, $J = 10.0$ Hz, 2 H), 4.66 (s, 1 H), 4.48 (s, 1 H), 4.35 (t, $J = 8.8$ Hz, 1 H), 3.80 (s, 3 H), 3.79 (s, 6 H), 3.02 (s, 2 H); ^{13}C NMR (100 MHz, $CDCl_3$) δ 173.70, 167.72, 152.66, 148.26, 147.76, 137.13, 135.88, 134.79, 132.54, 129.34, 128.40, 127.30, 125.54, 124.10, 119.10, 111.52, 109.78, 108.02, 107.18, 102.88, 101.64, 73.91, 71.62, 60.76, 56.11, 45.67, 43.80, 38.94; HRMS-ESI (*m/z*): calcd for $C_{31}H_{27}NNaO_9$ $[M + Na]^+$ 580.1578, found 580.1576.

Biological activity

CCK-8 assay

Cells were seeded in 96-well plates and treated with either vehicle (DMSO) or compounds with a range of concentrations for 72 h at 37 °C. After that, the medium was removed, and 10 µl CCK-8 was added to each well for another 3 h at 37 °C. Cell viability was calculated by quantifying the absorbance at 450 nm. IC_{50} values were obtained by GraphPad Prism 6.

Cell cycle analysis

K562/VCR cells were seeded in 6-well plates and treated with either vehicle (DMSO) or compounds with a range of concentrations for 48 h at 37 °C. Then, the cells were harvested, washed with PBS and fixed with 70% ethanol at 4 °C overnight. The cells were stained by PI/RNase A. Finally, apoptotic cells were measured by FACScan flow cytometer.

Apoptosis analysis

K562/VCR cells were treated with either vehicle (DMSO) or compounds with a range of concentrations for 48 h at 37 °C. Then, cells were collected and then were stained by 5 μL Annexin V-APC and 5 μL 7-AAD for another 15 min at room temperature in the dark. After staining, cells were measured by Flow Cytometer.

Mitochondrial membrane potential analysis

K562/VCR cells were treated with either vehicle (DMSO) or compounds with a range of concentrations for 48 h at 37 °C. After treatment, the cells were harvested, further incubated with JC-1 dye for 20 min at room temperature. Finally, the cells were washed two times with PBS and monitored by using a flow cytometer.

Measurement of intracellular ROS generation

K562/VCR cells were treated with either vehicle (DMSO) or compounds with a range of concentrations for 24 h at 37 °C. After incubation, the cells were harvested, washed with PBS and incubated with 10 μM DCFH-DA at 37 °C in the dark for 20 min. Subsequently, the cells were washed with PBS, and the ROS was analyzed by flow cytometer.

Immunofluorescent analysis

K562/VCR cells were treated with either vehicle (DMSO) or compounds with a range of concentrations for 24 h at 37 °C. Then, the cells were fixed with 4% paraformaldehyde and blocked for 45 min. The cells were further blocked by goat serum at room temperature for 20 min. Next, the cells were incubated with the primary antibody (α-tubulin) overnight at 4 °C, washed three times with PBS, and incubated with the corresponding Alexa Fluor 488 labeled secondary antibody at room temperature for 1 h. Cell nuclei were stained by DAPI at room temperature for 5 min. The fluorescence images were visualized using a fluorescence microscopy.

Molecular modeling

The molecular docking study was investigated using Schrödinger. The X-ray crystal structure of tubulin (PDB code 1SA0) was downloaded from the RCSB Protein Data Bank and prepared with Protein Prepared Wizard. The small molecule (**In-9**) was initially energy-minimized with using the LigPrep module and docked into colchicine binding site using Glide in Schrödinger. The figure of molecular modeling was visualized by using PYMOL.

Molecular dynamics simulation

The complex was studied by molecular dynamics simulations using the Amber16 software package. The ligand was assigned AM1-BCC charges and gaff2 atom types using antechamber. Simulation was carried out using the GPU accelerated PMEMD program with Amber ff14SB force field in periodic boundary conditions. The complex were immersed in a truncated octahedron box of TIP3P water molecules with a margin distance of 12.0 Å. The solvated box was further neutralized with Na^+ counter ions using the tLEAP program. Particle Mesh Ewald (PME) was employed to calculate the long-range electrostatic interactions, and the non-bonded energy cutoff was set to 10.0 Å. In order to remove any steric conflicts induced during system setup, structural optimizations were first performed on the relaxed water molecules and counter ions in two steps with the harmonic constraint potential of 10.0 kcal/mol•Å2 on all heavy atoms of both protein and ligands. Afterwards, the whole system was minimized without any restraint. The above steps were all executed by 2500 cycles of steepest descent minimization followed by 5000 cycles of conjugate gradient minimization. After system optimization, running of MD simulations was started on the system by gradually heating the system in the NVT ensemble from 0 to 298.15 K for 500 ps using a Langevin thermostat with a coupling coefficient of 5.0/ps and with a force constant of 10.0 kcal/mol•Å2 on the complex. And then 500 ps of density equilibration with a force constant of 10.0 kcal/mol•Å2 on the complex was performed. Subsequently, the system was again equilibrated for 500 ps by releasing all the restraints. Finally, production run for 40 ns MD simulations were performed under a constant temperature of 298.15 K in the NPT ensemble with periodic boundary conditions.

Western blotting

After treatment, total protein was extracted, and protein concentration was determined using the BCA Protein Assay Kit. The protein samples were separated by 10% sodium dodecyl sulfate-polyacrylamide electrophoresis gels (SDS-

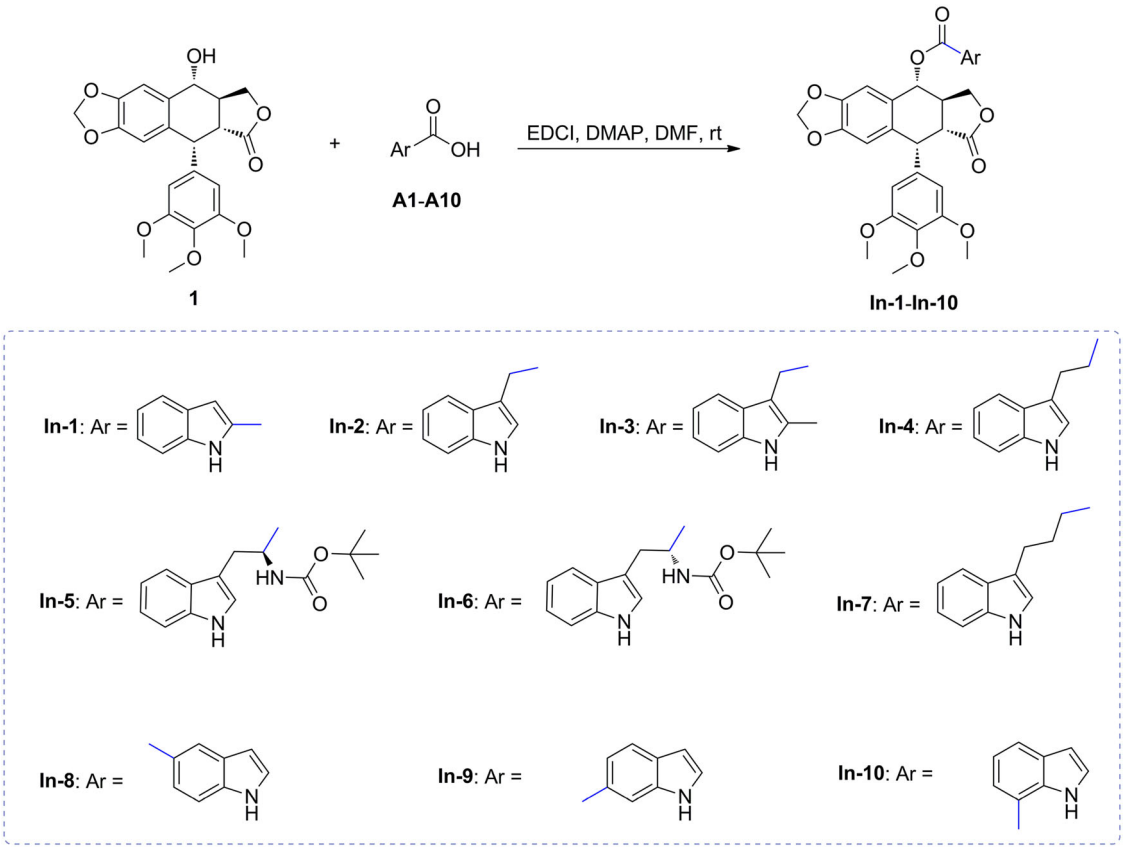

Scheme 1 Synthesis of indole carboxylic acid esters of podophyllotoxin

PAGE) and transferred to nitrocellulose membranes. The membranes were blocked with 5% fat-free dry milk for 2 h at room temperature and further incubated with the primary antibodies: CDK1, CDK2, Cleaved caspase3, Beclin1, LC3, P-gp, MRP1, p-AMPK, p-ERK1/2, p-JNK, p-P38, p-PI3K, p-AKT, p-mTOR, and β-actin overnight at 4 °C. Then, the membranes were treated with secondary antibodies for 2 h. All the membranes were visualized with ECL-detecting reagents.

SwissADME analysis

SwissADME analysis online was conducted for the prediction of the ADME parameters (http://www.swissadme.ch/).

Results and discussion

Chemistry

The synthetic approach for the preparation of indole carboxylic acid esters of podophyllotoxin (**In-1-In-10**) was illustrated in Scheme 1. The designed molecules were prepared using EDCI as coupling agent by reacting podophyllotoxin (**1**) with an appropriate indole carboxylic acid (**A1-A10**) in the presence of EDCI and DMAP in DMF at room temperature. The products were further purified using flash chromatography, and their structures were fully identified by ^{1}H and ^{13}C NMR spectrometry and high-resolution mass spectra (HRMS).

Biological activity

In vitro antiproliferative activity

The antiproliferative effect of the synthesized indole carboxylic acid esters of podophyllotoxin against drug-sensitive and -resistant human leukemia cells (K562 and K562/VCR) were measured by using the CCK-8 assay in vitro, while podophyllotoxin (**1**), etoposide (**2**), and vincristine (VCR) were used as the positive controls. The results (IC_{50} values) were summarized in Table 1. According to the data, almost all of compounds showed potent antiproliferative activity with submicromolar IC_{50} values against above two cell lines. Among these compounds, **In-2**, **In-8**, and **In-9**, which contained short linker or small substituent at the indole-ring, showed better

antineoplastic activity against K562 cells, with IC_{50} values of 0.043 ± 0.004, 0.081 ± 0.004, and 0.100 ± 0.008 μM, respectively, as well as K562/VCR cells, with IC_{50} values of 0.202 ± 0.055, 0.229 ± 0.012, and 0.227 ± 0.011 μM, respectively. However, a sharply decline of inhibitory activity was observed when longer linker or bigger substituent was introduced into the indole-ring, such as compounds **In-5**, **In-6**, and **In-7**. Interestingly, high cytotoxicity was found for the compounds bearing carboxyl group at position 5/6 at the indole-ring, such as **In-8** or **In-9**, instead of **In-1** or **In-10** containing carboxyl group at position 2/7.

In addition, several compounds, such as **In-8** and **In-9**, not only showed good activity, but also displayed low resistance factor (RF). For example, **In-9** possessed an IC_{50} value of 0.227 ± 0.011 μM against K562/VCR cells, which was 52.158- and 20.867-fold stronger than that of etoposide and VCR, respectively. Meanwhile, **In-9** had a lower RF value of 2.270, indicating that **In-9** might have the potential to reverse the MDR of K562/VCR cells.

Table 1 Antiproliferative activity

Compound	IC_{50} (μM)[a]		RF[b]
	K562	K562/VCR	
In-1	0.206 ± 0.008	0.292 ± 0.025	1.417
In-2	0.043 ± 0.004	0.202 ± 0.055	4.697
In-3	0.513 ± 0.102	1.221 ± 0.059	2.380
In-4	0.373 ± 0.036	0.589 ± 0.034	1.579
In-5	0.395 ± 0.022	1.291 ± 0.064	3.268
In-6	1.702 ± 0.054	1.768 ± 0.042	1.038
In-7	0.437 ± 0.012	0.619 ± 0.076	1.416
In-8	0.081 ± 0.004	0.229 ± 0.012	2.827
In-9	0.100 ± 0.008	0.227 ± 0.011	2.270
In-10	0.225 ± 0.018	0.472 ± 0.068	2.097
1[c]	0.025 ± 0.003	0.050 ± 0.004	2.000
2[c]	0.764 ± 0.104	11.840 ± 0.066	15.497
VCR[c]	0.178 ± 0.006	4.737 ± 0.647	26.612

[a]Data were expressed as mean $IC_{50} \pm SD$ (μM)

[b]RF was computed as IC_{50} (K562/VCR)/IC_{50} (K562)

[c]Literature values (Wang et al. 2018)

Measurement of intracellular ROS generation

Reactive oxygen species (ROS) have been shown to play important roles in multiple important biological processes, such as cell death and apoptosis (Valentini et al. 2009). To investigate whether the indole carboxylic acid esters of podophyllotoxin were able to generate ROS, we further used the oxidation sensitive fluorescent DCFH-DA to detect the intracellular ROS accumulation in K562/VCR cells. Cells were treated with vehicle, 0.25 μM **In-9** or 0.5 μM **In-9** for 24 h, stained with DCFH-DA, and analyzed by flow cytometry. As shown in Fig. 4, ROS level increased to 32.36% and 47.12% after treatment with 0.25 μM and 0.5 μM **In-9**, respectively, as compared with the vehicle-treated group (1.30%). These results showed that **In-9** had the high intracellular ROS-generating ability.

Immunofluorescent analysis

To investigate the effect of **In-9** on the microtubule polymerization, we further examined its ability to alter the cellular microtubule network of K562/VCR cells using immunofluorescence assay. Cells were treated with vehicle, 0.25 μM **In-9** or 0.5 μM **In-9** for 24 h, stained with anti-α-tubulin conjugated with FITC (green), counterstained with DAPI (blue), and then analysed by fluorescence microscope. In Fig. 5, we observed that the vehicle-treated cells exhibited a normal arrangement and organization of microtubules. In contrast, after 24 h of treatment, **In-9** almost disrupted the microtubule network in K562/VCR cells at a low concentration of 0.5 μM.

Molecular modeling

To rationalize the obtained experimental results, molecular docking studies of **In-9** were carried out into the colchicine

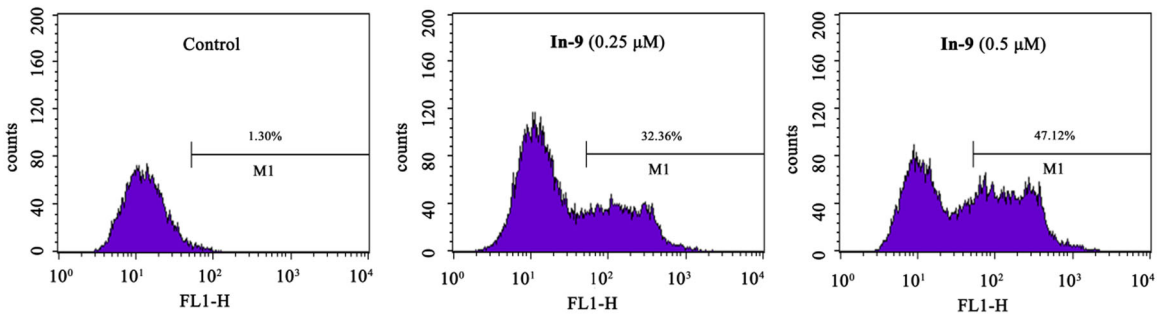

Fig. 4 Effect of **In-9** on reactive oxygen species. K562/VCR cells were incubated with vehicle, 0.25 μM **In-9** or 0.5 μM **In-9** for 24 h, and treated with DCFH-DA. The fluorescence was detected by using flow cytometer

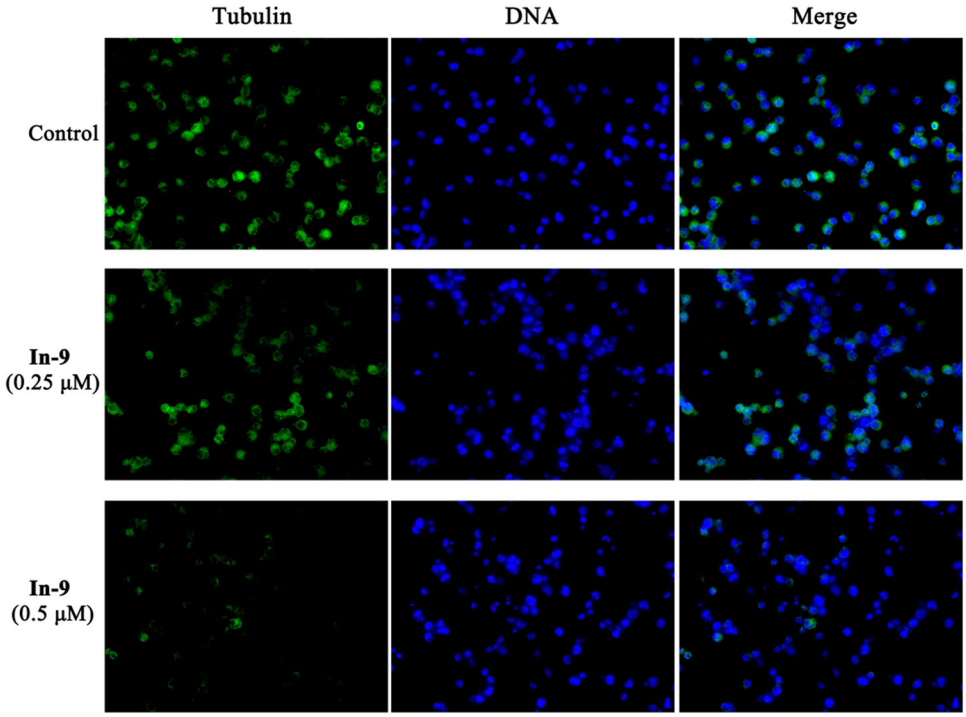

Fig. 5 Compound **In-9** interfered microtubule polymerization. K562/VCR cells were incubated with vehicle, 0.25 μM **In-9** or 0.5 μM **In-9** for 24 h, then stained with anti-a-tubulin conjugated with FITC (green) followed by DAPI (blue). Magnification ×400

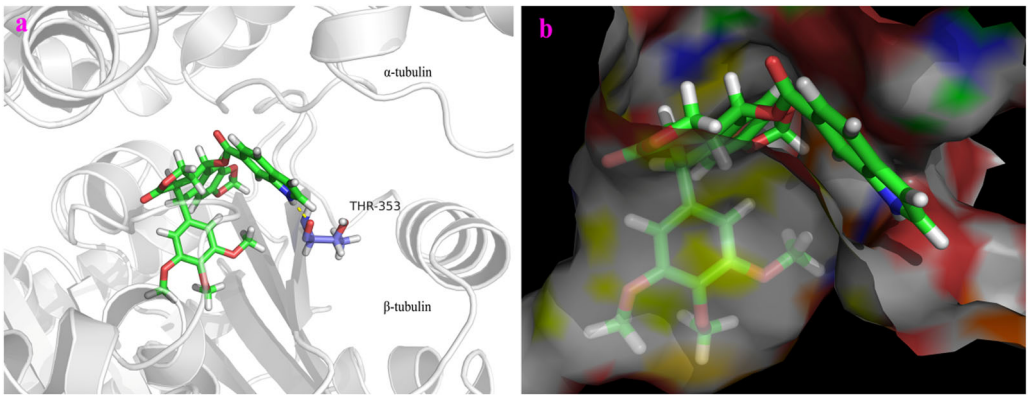

Fig. 6 The binding mode of compound **In-9** (green color stick) in the colchicine site of tubulin (PDB ID: 1SA0). The docking pose was illustrated by two different visualizations: **a** (ribbon) and **b** (protein surface) representations. Yellow dashed line represents hydrogen bond

binding site of tubulin crystal structure (PDB code: 1SA0) by using GLIDE docking module of Schrödinger suite, and analyzed by PYMOL software. From the results, it was observed that 3,4,5-trimethoxybenzoyl at ring-E of **In-9** were well accommodated and located deeply inside the colchicine binding site of the β-tubulin (Fig. 6). Meanwhile, the ring of indole was located into the narrow gap between the α-subunit and β-subunit, instead of the hydrophobic cavity of α-Tubulin, and established a hydrogen bond with THR-353 residue ($d = 2.1$ Å) belonging to the β-subunit of tubulin. Overall, it was found that compound **In-9** displayed antiproliferative activity by occupying the colchicine binding site of the tubulin.

Molecular dynamics simulation

In order to further exam the reliability of our docking result and prove the stability of the complex of **In-9** and tubulin, 40 ns molecular dynamics (MD) simulation studies were performed by using the Amber16. The root mean square deviation (RMSD) plot of protein-ligand complex during the MD simulations was seen in Fig. 7. The simulation

results revealed that the RMSD tended to be stable, which indicated that the structure of the complex of **In-9** and tubulin was basically in a stable state.

Cell cycle analysis

Based on the effect of **In-9** on the microtubule polymerization, we further examined its effect on the cell cycle progression of K562/VCR cells using flow cytometry. Cells were treated with vehicle, 0.25 μM **In-9** or 0.5 μM **In-9** for 48 h, and then stained with propidium iodide (PI) followed by flow cytometric analysis. As shown in Fig. 8, after incubation with **In-9** at the concentrations of 0.25 and 0.5 μM, the percentages of cells in the G2 increased to 54.30% and 60.20%, respectively, while there was only 7.87% in the control group. These results showed that compound **In-9** was effective in arresting the cell cycle at the G2 phase, which was consistent with other tubulin inhibitors.

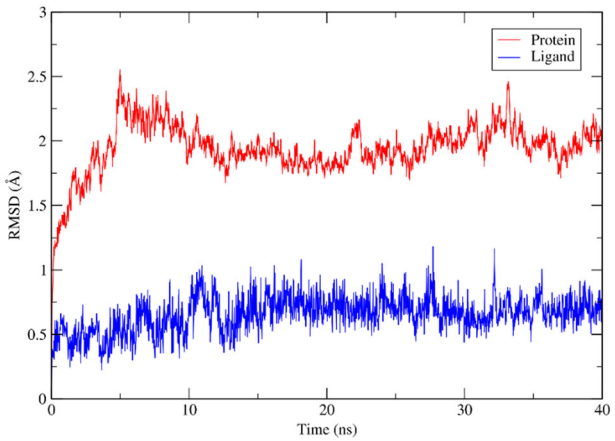

Fig. 7 Molecular dynamics simulation trajectory analysis of **In-9** with tubulin. RMSD value plot of the protein-ligand complex

Apoptosis analysis

The apoptosis inducing effect of **In-9** on K562/VCR cells was further investigated by using annexin V-FITC/PI staining assay. Cells were treated with vehicle, 0.25 μM **In-9** or 0.5 μM **In-9** for 48 h, and stained with Annexin V-FITC and PI followed by flow cytometric analysis. As depicted in Fig. 9, K562/VCR cells treated with **In-9** at the concentrations of 0.25 and 0.5 μM displayed an accumulation of apoptotic cells from 6.10% (untreated control) to 30.63 and 55.65%, respectively. These results indicated that **In-9** exerted the antiproliferative activity through the induction of cell apoptosis.

Mitochondrial membrane potential analysis

The mitochondrial membrane potential (MMP), generated by proton pumps, is necessary for mitochondrial functioning. Previous reports indicate that the loss of MMP might be an early event of apoptosis (Martínez-Reyes et al. 2016). Thus, the effect of compound **In-9** on MMP was investigated by staining with fluorescent dye JC-1. K562/VCR cells were treated with vehicle, 0.25 μM **In-9** or 0.5 μM **In-9** for 48 h, stained with JC-1, and then analysed by flow cytometry. As seen in Fig. 10, cells incubated with 0.25 and 0.5 μM **In-9** displayed 30.78 and 47.73% reduction of MMP, respectively, as compared with the control group (6.29%). The results suggested that **In-9** could lead to the

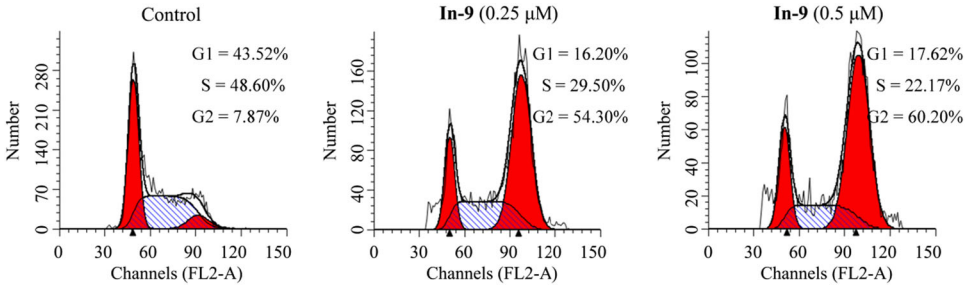

Fig. 8 Compound **In-9** induced cell cycle arrest. K562/VCR cells were incubated with vehicle, 0.25 μM **In-9** or 0.5 μM **In-9** for 48 h

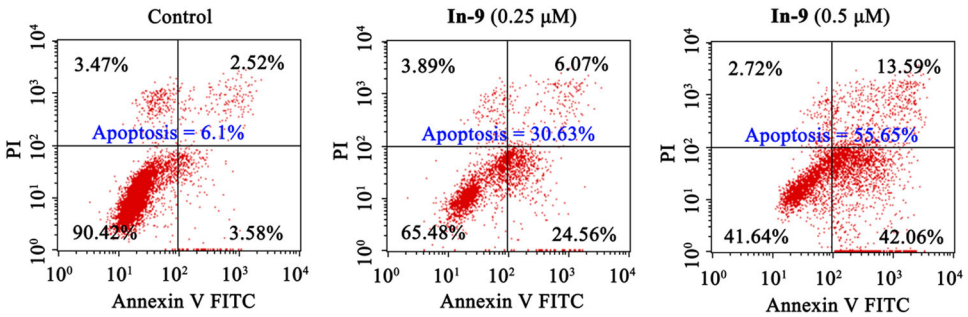

Fig. 9 Pro-apoptotic effect of compound **In-9**. K562/VCR cells were incubated with vehicle, 0.25 μM **In-9** or 0.5 μM **In-9** for 48 h

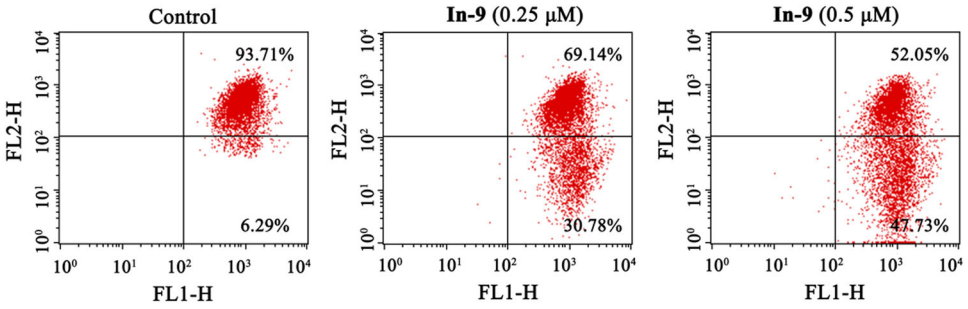

Fig. 10 Effects of compound **In-9** on mitochondrial membrane potential. K562/VCR cells were incubated with vehicle, 0.25 μM **In-9** or 0.5 μM **In-9** for 48 h, followed by incubation with the JC-1 dye

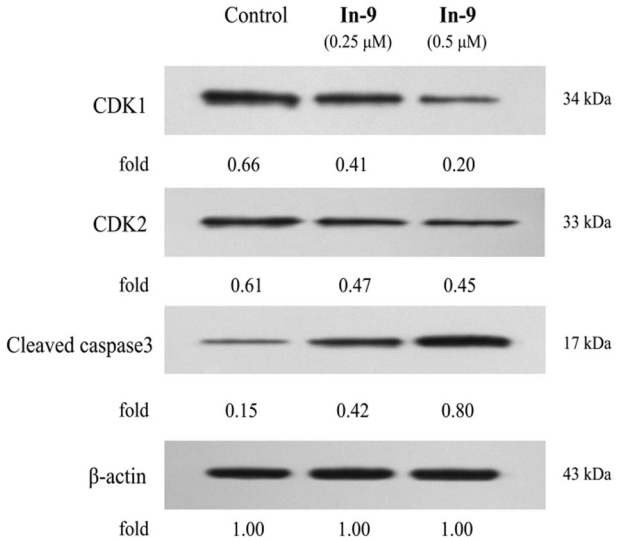

Fig. 11 Effects of compound **In-9** on the levels of CDK1, CDK2, and Cleaved caspase3. K562/VCR cells were incubated with vehicle, 0.25 μM **In-9** or 0.5 μM **In-9** for 48 h, and then analyzed by western blotting

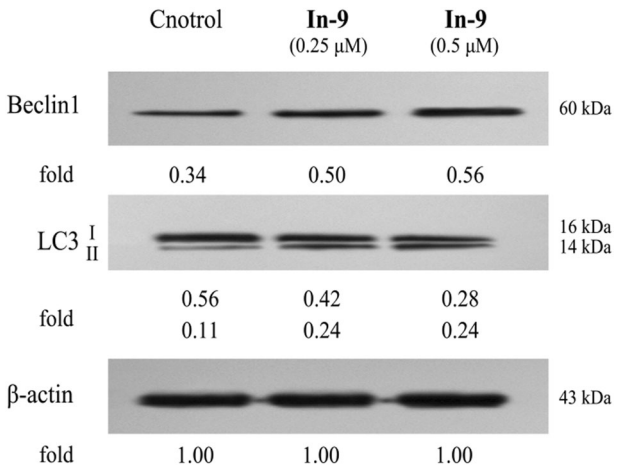

Fig. 12 Effects of compound **In-9** on the levels of Beclin1 and LC3. K562/VCR cells were incubated with vehicle, 0.25 μM **In-9** or 0.5 μM **In-9** for 48 h, and then analyzed by western blotting

loss of MMP, which may trigger apoptosis in the early period.

Western blotting

Cyclin-dependent kinases (CDKs) and caspases are crucial in the progress of cycle arrest and apoptosis, respectively (Yi et al. 2015). Thus, to further explore the underlying mechanisms of cycle arrest and apoptosis induced by **In-9**, we measured the expression levels of CDK1, CDK2, and Cleaved caspase3 in **In-9**-treated K562/VCR cancer cells by western blot assays. Cells were treated with vehicle, 0.25 μM **In-9** or 0.5 μM **In-9** for 48 h, and then detected by western blot. As shown in Fig. 11, treatment with **In-9** (0.25 or 0.5 μM) significantly reduced the levels of CDK1 and CDK2 in K562/VCR cells, as compared with that in the control groups. Moreover, **In-9** (0.25 or 0.5 μM) was observed to trigger the activation of caspase3 as compared with the control. These results suggested that the cycle arrest and apoptosis induced by **In-9** were at least partially mediated through inhibition of CDKs, and activation of caspase, respectively.

Autophagy, a conserved catabolic process, had two different roles, pro-death and pro-survival, which were depended on the cell type and extracellular context (Levy et al. 2017). In order to confirm the role of autophagy in **In-9** induced K562/VCR cells death, we further measured the Beclin1 and LC3-II levels using western blot. Cells were treated with vehicle, 0.25 μM **In-9** or 0.5 μM **In-9** for 48 h, and then detected by western blot. As shown in Fig. 12, the levels of Beclin1 were significantly increased by **In-9** in K562/VCR cells. Meanwhile, we observed that LC3-II protein (cleavage of LC3) levels markedly increased after **In-9** treatment, which was a hallmark of autophagy and produced during autophagosome formation. Altogether, these data showed that **In-9** could activate autophagy in resistant K562/VCR cells.

In CCK-8 assay, it was found that **In-9** had a lower RF value of 2.270, indicating that **In-9** might have the potential to reverse the MDR of K562/VCR cells. To further evaluate the mechanism of anti-MDR effects of **In-9**, the levels of two MDR-related proteins, P-glycoprotein (P-gp) and MDR protein 1 (MRP1), in K562/VCR cells were measured by western blotting. Cells were treated with vehicle, 0.25 μM **In-9** or 0.5 μM **In-9** for 48 h, and then detected by western

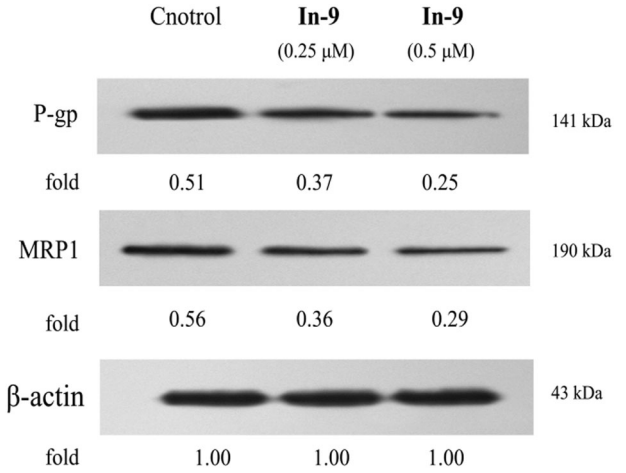

Fig. 13 Effects of compound **In-9** on the levels of P-gp and MRP1. K562/VCR cells were incubated with vehicle, 0.25 μM **In-9** or 0.5 μM **In-9** for 48 h, and then analyzed by western blotting

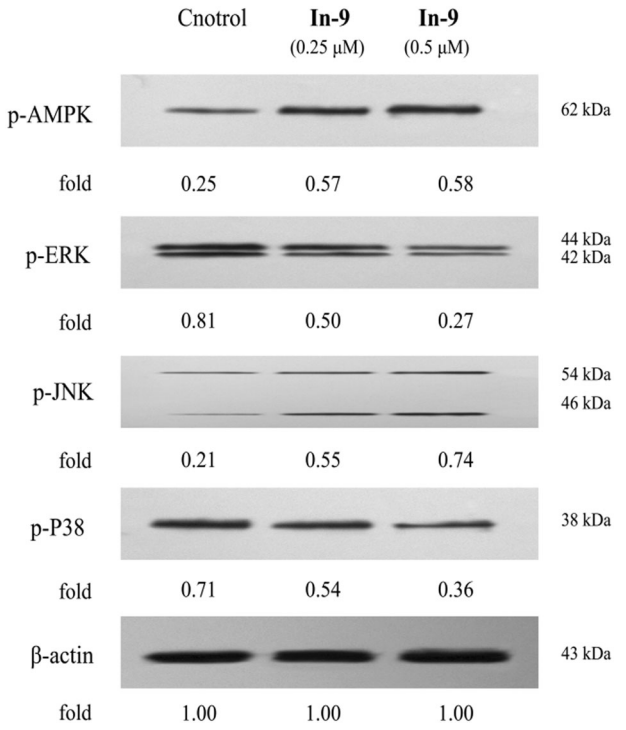

Fig. 14 Effects of compound **In-9** on the AMPK and MAPK signaling. K562/VCR cells were incubated with vehicle, 0.25 μM **In-9** or 0.5 μM **In-9** for 48 h, and then analyzed by western blotting

blot. As shown in Fig. 13, a decrease in P-gp and MRP1 protein levels was observed in **In-9**-exposed K562/VCR cells as compared with the control cells. Our findings confirmed that **In-9** exhibited the anti-MDR ability via downregulating the levels of P-gp and MRP1 proteins.

It is well known that AMP-activated protein kinase (AMPK), activated by a decrease in ATP levels, is involved in autophagy induction (Mihaylova and Shaw 2011). In

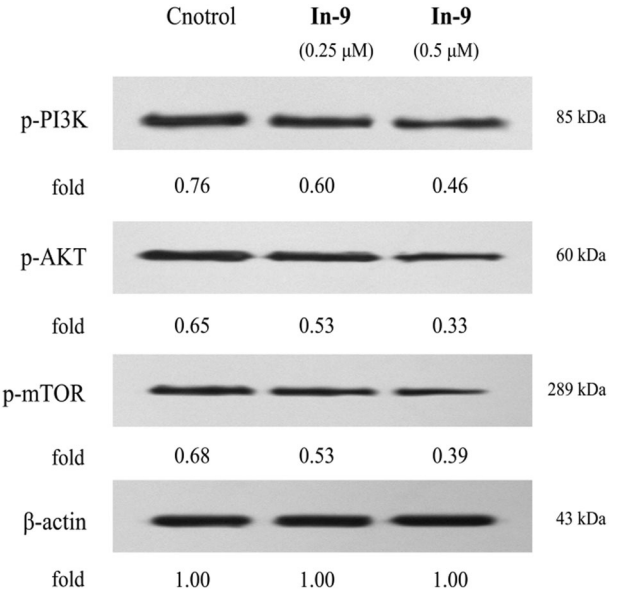

Fig. 15 Effects of compound **In-9** on the PI3K/AKT/mTOR signaling. K562/VCR cells were incubated with vehicle, 0.25 μM **In-9** or 0.5 μM **In-9** for 48 h, and then analyzed by western blotting

addition, the mitogen-activated protein kinase (MAPK) pathways, including extracellular signal-regulated kinases (ERK1/2), c-Jun-NH2-terminal kinases (JNK1/2) and p38, work in transmitting extracellular signals and play important roles in many physiological activities, such as autophagy (Sui et al. 2014). In present study, to further gain insights into the mechanisms underlying the activity of **In-9**, AMPK and MAPK pathways were selected to explore the autophagy regulatory mechanisms induced by **In-9** in K562/VCR cells. Cells were treated with vehicle, 0.25 μM **In-9** or 0.5 μM **In-9** for 48 h, and then determined by western blot. As shown in Fig. 14, treatment with **In-9** significantly enhanced the AMPK and JNK phosphorylation in K562/VCR cells, however, it dramatically inhibited phosphorylation of ERK and P38, when compared to the control. Therefore, **In-9** attenuated the AMPK and JNK signaling, but inhibited the ERK and P38 signaling in K562/VCR cancer cells, which might contribute to its antiproliferative activity. To the best knowledge of the authors, there is no study in the literature which reveals that podophyllotoxin or its derivative could activate the AMPK pathway in drug-resistant cancer cells.

PI3K/AKT/mTOR pathway is crucial for migration, autophagy, and drug resistance of cancer cells (LoPiccolo et al. 2008; Polivka and Janku 2014). To further unravel the underlying molecular mechanism of **In-9**, western blotting experiments were performed to examine the regulatory effects of **In-9** on the PI3K/AKT/mTOR pathway in K562/VCR cells. Cells were treated with vehicle, 0.25 μM **In-9** or 0.5 μM **In-9** for 48 h, and then determined by western blot. Figure 15 showed that treatment with **In-9** decreased the

Table 2 Various parameters obtained from SwissADME online

Compound	MW (g/mol) NMT[b] 500	HBDs NMT[b] 5	HBAs NMT[b] 10	mLogP[a] NMT[b] 5	Druglikeness Lipinski
In-9	557.55	1	9	2.60	Yes (1 violation)

[a]*mLogP* logarithm of the octanol-water partition coefficient

[b]*NMT* Not more than

levels of phosphorylation of PI3K, AKT, and mTOR in K562/VCR cancer cells, indicating that **In-9** could inhibit the PI3K/AKT/mTOR pathway. mTOR, a key regulator of autophagy, is the major inhibitory signal of autophagy in the presence of abundant nutrients and growth factors (Levine and Kroemer 2008). And PI3K/AKT is reported to be the major up-stream regulator of mTOR, which responds to many growth factors (Lum et al. 2005). Several recent studies have shown the negative regulation of autophagy by the PI3K/AKT/mTOR signaling pathway. For example, Saiki et. al found caffeine increased autophagic levels via suppression of the PI3K/AKT/mTOR signaling pathway (Saiki et al. 2011). Rottlerin, a polyphenol product isolated from *Mallotus philippensis*, was observed to induce autophagy via inhibition of PI3K/AKT/mTOR pathway in human pancreatic cancer stem cells (Singh et al. 2012). Consistent with above literature results, in the present study, we found that **In-9** could induce autophagy through inhibition of the PI3K/AKT/mTOR signaling pathway.

Prediction of druglikeness of In-9 by Lipinski's rule of five

To predict the druglikeness property of compound **In-9**, the calculated values of parameters of Lipinski's rule of five were analysed online by using the web tool SwissADME. As shown in Table 2, **In-9** had less than 5 hydrogen bond donors (HBDs), less than 10 hydrogen bond acceptors (HBAs) and mLogP < 5, except molecular weight (557.55), which slightly exceeded 500. The predicted results by SwissADME suggested that compound **In-9** might have drug like behavior.

Conclusions

In summary, a series of indole carboxylic acid esters of podophyllotoxin were synthesized and biologically evaluated. It was found that compound **In-9** showed strong antiproliferative activity against both drug-sensitive K562, and drug-resistant K562/VCR cells. Furthermore, **In-9** promoted intracellular ROS accumulation, induced apoptosis and cycle arrest at the G2 phase, and disrupted the microtubule network in K562/VCR cells. Additionally, **In-9** exhibited the anti-MDR ability, attenuated the AMPK and JNK signaling, and inhibited the ERK, P38, and PI3K/AKT/mTOR signaling in K562/VCR cells. In silico prediction revealed that **In-9** possessed good ADME parameters. Together, these results indicated that **In-9**, a hybrid of indole carboxylic acid and podophyllotoxin, had potent anticancer activity against resistant leukemia cancer. Our findings indicated that **In-9** might be a promising candidate for the drug-resistant leukemia cancer.

Acknowledgements This work was financially supported by the National Natural Science Foundation of China (81860622), Department of Science and Technology of Guizhou Province ([2017]1219), Joint Fund of the Department of Science and Technology of Zunyi City and Zunyi Medical University ([2018]27), and National First-Rate Construction Discipline of Guizhou Province (Pharmacy) (YLXKJS-YX-04).

Compliance with ethical standards

Conflict of interest The authors declare that they have no conflict of interest.

References

Aller SG, Yu J, Ward A, Weng Y, Chittaboina S, Zhuo R, Harrell PM, Trinh YT, Zhang Q, Urbatsch IL, Chang G (2009) Structure of P-glycoprotein reveals a molecular basis for poly-specific drug binding. Science 323:1718–1722

Bailly C (2012) Contemporary challenges in the design of topoisomerase II inhibitors for cancer chemotherapy. Chem Rev 112:3611–3640

Baldwin EL, Osheroff N (2005) Etoposide, topoisomerase II and cancer. Curr Med Chem 5:363–372

Binkhathlan Z, Lavasanifar A (2013) P-glycoprotein inhibition as a therapeutic approach for overcoming multidrug resistance in cancer: current status and future perspectives. Curr Cancer Drug Targets 13:326–346

Bommagani S, Ponder J, Penthala NR, Janganati V, Jordan CT, Borrelli MJ, Crooks PA (2017) Indole carboxylic acid esters of melampomagnolide B are potent anticancer agents against both hematological and solid tumor cells. Eur J Med Chem 136:393–405

Cao B, Chen H, Gao Y, Niu C, Zhang Y, Li Y (2015) CIP-36, a novel topoisomerase II-targeting agent, induces the apoptosis of multidrug-resistant cancer cells in vitro. Int J Mol Med 35:771–776

Chen H, Bi W, Cao B, Yang Z, Chen S, Shang H, Yu P, Yang J (2010) A novel podophyllotoxin derivative (YB-1EPN) induces apoptosis and down-regulates express of P-glycoprotein in multidrug resistance cell line KBV200. Eur J Pharmacol 627:69–74

Cheng WH, Cao B, Shang H, Niu C, Zhang LM, Zhang ZH, Tian DL, Zhang S, Chen H, Zhou ZM (2014) Synthesis and evaluation of novel podophyllotoxin derivatives as potential antitumor agents. Eur J Med Chem 85:498–507

Dadashpour S, Emami S (2018) Indole in the target-based design of anticancer agents: a versatile scaffold with diverse mechanism. Eur J Med Chem 150:9–29

Gottesman MM (2002) Mechanisms of cancer drug resistance. Annu Rev Med 53:615–627

Han HW, Qiu HY, Hu C, Sun WX, Yang RW, Qi JL, Wang XM, Lu GH, Yang YH (2016) Design, synthesis and anti-cancer activity evaluation of podophyllotoxin-norcantharidin hybrid drugs. Bioorg Med Chem Lett 26:3237–3242

Kamal A, Ali Hussaini SM, Rahim A, Riyaz S (2015) Podophyllotoxin derivatives: a patent review (2012-2014). Expert Opin Ther Pat 25:1025–1034

Kathawala RJ, Gupta P, Ashby CR, Chen ZS (2015) The modulation of ABC transporter-mediated multidrug resistance in cancer: a review of the past decade. Drug Resist Update 18:1–17

Kim SY, Ryu JS, Li H, Park WJ, Yun HY, Beak KJ, Kwon NS, SOHN UD, Kim DS (2010) UVB-activated indole-3-acetic acid induces apoptosis of PC-3 prostate cancer cells. Anticancer Res 30:4607–4612

Lai JL, Liu YH, Liu C, Qi MP, LIu RN, Zhu XF, Zhou QG, Chen YY, Guo AZ, Hu CM (2017) Indirubin inhibits LPS-induced inflammation via TLR4 abrogation mediated by the NF-kB and MAPK signaling pathways. Inflammation 40:1–12

Leneva IA, Russell RJ, Boriskin YS, Hay AJ (2009) Characteristics of arbidol-resistant mutants of influenza virus: implications for the mechanism of anti-influenza action of arbidol. Antivir Res 81:132–140

Levine B, Kroemer G (2008) Autophagy in the pathogenesis of disease. Cell 132:27–42

Levy JMM, Towers CG, Thorburn A (2017) Targeting autophagy in cancer. Nat Rev Cancer 17:528–542

Li W, Zhang H, Assaraf YG, Zhao K, Xu X, Xie J, Yang DH, Chen ZS (2016) Overcoming ABC transporter-mediated multidrug resistance: Molecular mechanisms and novel therapeutic drug strategies. Drug Resist Update 27:14–29

Liu X, Zhang LL, Xu XH, Hui L, Zhang JB, Chen SW (2013) Synthesis and anticancer activity of dichloroplatinum (II) complexes of podophyllotoxin. Bioorg Med Chem Lett 23:3780–3784

LoPiccolo J, Blumenthal GM, Bernstein WB, Dennis PA (2008) Targeting the PI3K/Akt/mTOR pathway: effective combinations and clinical considerations. Drug Resist Update 11:32–50

Lum JJ, Bauer DE, Kong M, Harris MH, Li C, Lindsten T, Thompson CB (2005) Growth factor regulation of autophagy and cell survival in the absence of apoptosis. Cell 120:237–248

Martínez-Reyes I, Diebold LP, Kong H, Schieber M, Huang H, Hensley CT, Mehta MM, Wang T, Santos JH, Woychik R, Dufour E, Spelbrink JN, Weinberg SE, Zhao Y, DeBerardinis RJ, Chandel NS (2016) TCA cycle and mitochondrial membrane potential are necessary for diverse biological functions. Mol Cell 61:199–209

Merzouki A, Buschmann MD, Jean M, Young RS, Liao S, Gal S, Li Z, Slilaty SN (2012) Adva-27a, a novel podophyllotoxin derivative found to be effective against multidrug resistant human cancer cells. Anticancer Res 32:4423–4432

Mihaylova MM, Shaw RJ (2011) The AMPK signalling pathway coordinates cell growth, autophagy and metabolism. Nat Cell Biol 13:1016–1023

Mishra S, Singh P (2016) Hybrid molecules: the privileged scaffolds for various pharmaceuticals. Eur J Med Chem 124:500–536

Polivka Jr J, Janku F (2014) Molecular targets for cancer therapy in the PI3K/AKT/mTOR pathway. Pharmacol Ther 142:164–175

Romero DL, Olmsted RA, Poel TJ, Morge RA, Biles C, Keiser BJ, Kopta LA, Friis JM, Hosley JD, Stefanski KJ, Wishka DG, Evans DB, Morris J, Stehle RG, Sharma SK, Yagi Y, Voorman RL, Adams WJ, Tarpley WG, Thomas RC (1996) Targeting delavirdine/atevirdine resistant HIV-1: identification of (alkylamino) piperidine-containing bis(heteroaryl)piperazines as broad spectrum HIV-1 reverse transcriptase inhibitors. J Med Chem 39:3769–3789

Saiki S, Sasazawa Y, Imamichi Y, Kawajiri S, Fujimaki T, Tanida I, Kobayashi H, Sato F, Sato S, Ishikawa KI, Imoto M, Hattori N (2011) Caffeine induces apoptosis by enhancement of autophagy via PI3K/Akt/mTOR/p70S6K inhibition. Autophagy 7:176–187

Shukla S, Wu CP, Ambudkar SV (2008) Development of inhibitors of ATP-binding cassette drug transporters-present status and challenges. Expert Opin Drug Metab Toxicol 4:205–223

Singh BN, Kumar D, Shankar S, Srivastava RK (2012) Rottlerin induces autophagy which leads to apoptotic cell death through inhibition of PI3K/Akt/mTOR pathway in human pancreatic cancer stem cells. Biochem Pharmacol 84:1154–1163

Stone RM, Manley PW, Larson RA, Capdeville R (2018) Midostaurin: its odyssey from discovery to approval for treating acute myeloid leukemia and advanced systemic mastocytosis. Blood Adv 2:444–453

Sui X, Kong N, Ye L, Han W, Zhou J, Zhang Q, He C, Pan H (2014) p38 and JNK MAPK pathways control the balance of apoptosis and autophagy in response to chemotherapeutic agents. Cancer Lett 344:174–179

Szakács G, Paterson JK, Ludwig JA, Booth-Genthe C, Gottesman MM (2006) Targeting multidrug resistance in cancer. Nat Rev Drug Discov 5:219–234

Valentini A, Conforti F, Crispini A, De Martino A, Condello R, Stellitano C, Rotilio G, Ghedini M, Federici G, Bernardini S, Pucci D (2009) Synthesis, oxidant properties, and antitumoral effects of a heteroleptic palladium (II) complex of curcumin on human prostate cancer cells. J Med Chem 52:484–491

Wang J, Long L, Chen Y, Xu Y, Zhang L (2018) Design, synthesis and antineoplastic activity of novel hybrids of podophyllotoxin and indirubin against human leukaemia cancer cells as multifunctional anti-MDR agents. Bioorg Med Chem Lett 28:1817–1824

Wang ZZ, Sun WX, Wang X, Zhang YH, Qiu HY, Qi JL, Pang YJ, Lu GH, Wang XM, Yu FG, Yang YH (2017) Design, synthesis, biological evaluation, and 3D-QSAR analysis of podophyllotoxin-dioxazole combination as tubulin targeting anticancer agents. Chem Biol Drug Des 90:236–243

Yi X, Zhang X, Jeong H, Shin YM, Park DH, You S (2015) A novel bispidinone analog induces S-phase cell cycle arrest and apoptosis in HeLa human cervical carcinoma cells. Oncol Rep 33:1526–1532

You Y (2005) Podophyllotoxin derivatives: current synthetic approaches for new anticancer agents. Curr Pharm Des 11:1695–1717

Zhang L, Chen F, Zhang Z, Chen Y, Lin Y, Wang J (2016a) Design, synthesis and evaluation of the multidrug resistance-reversing activity of pyridine acid esters of podophyllotoxin in human leukemia cells. Bioorg Med Chem Lett 26:4466–4471

Zhang L, Liu L, Zheng C, Wang Y, Nie X, Shi D, Chen Y, Wei G, Wang J (2017a) Synthesis and biological evaluation of novel podophyllotoxin-NSAIDs conjugates as multifunctional anti-MDR agents against resistant human hepatocellular carcinoma Bel-7402/5-FU cells. Eur J Med Chem 131:81–91

Zhang L, Liu L, Zheng C, Wang Y, Wang J, Yao Q (2017b) Synthesis of novel indirubin derivatives and their effects on the proliferation, cell cycle and apoptosis in acute myeloblastic leukemia HL-60 cells. Chin J Org Chem 37:1523–1529

Zhang L, Zhang Z, Chen F, Chen Y, Lin Y, Wang J (2016b) Aromatic heterocyclic esters of podophyllotoxin exert anti-MDR activity in human leukemia K562/ADR cells via ROS/MAPK signaling pathways. Eur J Med Chem 123:226–235

Zhang L, Zheng J, Rong Y, Yang C, Long L, Xu Y, Chen Y, Wang J, Yao Q (2018) Synthesis, antitumor evaluation and molecular docking study of a novel podophyllotoxin-lonidamine hybrid. Med Chem Res 27:2231–2238